LatHyS global hybrid simulation of the BepiColombo second Venus flyby

Sae Aizawa, Moa Persson, Thibault Menez, Nicolas Andre, Ronan Modolo, Vincent Genot, Beatriz Sanchez-Cano, M. Volwerk, Jean-Yves Chaufray, Claire Baskevitch, et al.

LatHyS global hybrid simulation of the BepiColombo second Venus flyby

S. Aizawa [1],[2], M. Persson[1], T. Menez[1], N. André[1], R. Modolo[3], V. Génot[1], B. Sanchez-Cano[6], M. Volwerk[11], J-Y. Chaufray[3], C. Baskevitch[3], D. Heyner[7], Y. Saito[4], Y. Harada[10], F. Leblanc[3], A. Barthe[1], E. Penou[1], A. Fedorov[1], J.-A. Sauvaud[1], S. Yokota[5], U. Auster[7], I. Richter[7], J. Mieth[7], T. S. Horbury[8], P. Louarn[1], C. J. Owen[9], G. Murakami[4]

[1] IRAP, CNRS-UPS-CNES, Toulouse, France

[2] Graduate School of Science, Tohoku University, Sendai, Japan

[3] LATMOS/IPSL, UVSQ Université Paris-Saclay, UPMC University Paris CNRS, Guyancourt, France

[4] Institute of Space and Astronautical Science, Japan Aerospace Exploration Agency, Japan

[5] Department of Earth and Space Science, Graduate School of Science, Osaka University, Japan

[6] School of Physics and Astronomy, University of Leicester, Leicester, UK

[7] Institute for Geophysics and Extraterrestrial Physics, Technische Universität Braunschweig, Braunschweig, Germany

[8] Imperial College London, South Kensington Campus, London, UK

[9] Mullard Space Science Laboratory, University College London, Holmbury St. Mary, Dorking, Surrey, RH5 6NT, UK

[10] Department of Geophysics, Graduate School of Science, Kyoto University, Kyoto, Japan

[11] Space Research Institute, Austrian Academy of Sciences, Graz, Austria

Keywords: BepiColombo; Global hybrid simulation; Venus flyby; Solar Orbiter

Abstract

Plasma and magnetic field observations by BepiColombo during its 2nd Venus flyby in August, 10 2021 have been examined and compared with the newly developed global hybrid

simulation LatHyS for the Venusian environment. The LatHyS-Venus simulation was first validated by a comparison with Venus Express observations obtained during average solar wind conditions, before it was applied to the BepiColombo flyby using as inputs solar wind parameters measured upstream of Venus by Solar Orbiter. The simulation confirms that BepiColombo passed through the stagnation region of Venus, which supports the results obtained by data analysis. In addition, we have sampled the plasma parameters along the BepiColombo trajectory and constructed the energy spectrum for two species, i.e., protons of both solar wind and planetary origin, and planetary oxygen ions, and discussed the possible effects due to the limited field of views of the plasma instruments onboard BepiColombo. The most intense observational features are properly captured in the LatHyS-Venus simulation, which show that the model is a powerful tool for interpreting and understanding in-situ data obtained from the instruments with a limited field of views. The estimated ion escape for protons and oxygen ions at Venus during the BepiColombo flyby is of the order of $\sim 10^{24}$ ions/s, which is the same order of magnitude compared to the estimation from Venus Express observations at the solar minimum.

1. Introduction

The absence of an intrinsic magnetic field at Venus indicates that the solar wind directly interacts with its ionosphere and upper atmosphere. This configuration gives birth to complex interaction regions whose structure and dynamics are governed by the prevailing solar wind conditions as well as the solar Extreme UltraViolet (EUV) irradiance. The solar wind interaction with Venus has been the subject of in-depth studies by several spacecraft in the history of space exploration [e.g., Futaana et al., 2017], notably by the 14-year long Pioneer Venus Orbiter (PVO) mission (1978-1992), and more recently by the Venus Express (VEX) mission which orbited around the planet from 2006 to 2014. These missions provided us with new insights into the evolution of planetary atmosphere and its escape to space, as well as on the physical processes operating in induced magnetospheres and ionospheres.

The wealth of data obtained by the PVO and VEX missions also encouraged the development of several numerical models describing the plasma interaction on scales ranging from ion gyro radius to the entire induced magnetosphere in order to understand the global context and physical settings of the observations at Venus. These include, among others, magnetohydrodynamic (MHD) models by McGray and Pontius (1994), Cable and Steinolfson (1995), De Zeeuw et al. (1996), Murawski and Steinolfson (1996a; 1996b), Tanaka and Murawski (1997), Kallio et al. (1998), Jin et al. (2008), Terada et al. (2009), Benna et al. (2009), and Ma et al. (2013; 2020), and hybrid models by Brecht and Ferrante (1991), Terada et al. (2002; 2004), Kallio et al. (2006; 2008; 2012), Jarvinen et al. (2008; 2009; 2013; 2016; 2020), Martinecz et al. (2008), Liu et al. (2009), and Brecht and Ledvina (2021). The MHD models are able to reproduce some of the global characteristics of the solar wind interaction with Venus but they do not take into account the particle behavior. Considering that the scale of the interaction region at Venus is close to the ion kinetic scale, and the presence of pickup ions from the exosphere, the hybrid models become important tools to properly understand the interaction between the solar wind plasma and the Venusian environment. Neutral species and planetary ions are implemented in hybrid models, but most of them rely on the use of simplified neutral atmospheres and exospheres, with no internal dynamics, and simplified ion production descriptions. Despite these limitations, the ion escape rates estimated by these models match very well with observations [e.g., Jarvinen et al., 2009].

Since Venus is an important target for swing-by maneuvers to reach the inner heliosphere (e.g., solar corona, Mercury), or the outer heliosphere, several flybys by spacecraft equipped with more sophisticated plasma and field instrumentation than the ones onboard PVO and VEX have or will occur in the recent or coming years (e.g., Parker Solar Probe, Solar Orbiter, BepiColombo, and JUICE). Whereas such flyby missions provide only snapshots of the Venusian environment, their unique geometry and instrumental capabilities have already enabled us to obtain new and unique observations related to, e.g., the substantial variation in the density and temperature of the Venusian ionosphere over the Solar Cycle during Parker Solar Probe 3rd flyby [Collinson et al., 2021a], the extent of a cold plasma tail ray in the Venusian wake during Parker Solar Probe 4th flyby [Collinson

et al., 2021b], or the nature of plasma waves and particle energization in the far distant tail region during Solar Orbiter 1st flyby [Allen et al., 2021; Hadid et al., 2021; Volwerk et al., 2021a] as well as during BepiColombo 1st flyby [Volwerk et al., 2021b].

Solar Orbiter and BepiColombo made their 2nd Venus flyby just 33 hours apart on 9 and 10 August 2021. This double flyby provided a rare opportunity for BepiColombo to study the Venusian plasma environment and its interaction with the solar wind using Solar Orbiter as a solar wind monitor located very close upstream of the induced magnetosphere of Venus. A similar configuration occurred during the final Venus flyby of MESSENGER when Venus Express was in orbit around the planet [Slavin et al., 2009]. This motivates us to compare the newly obtained observations by BepiColombo with the outputs of a hybrid model of the Venus-solar wind interaction which implements a more sophisticated exosphere and ion production compared to previous models.

In section 2 we describe the extension to the Venusian environment of the global hybrid code LatHyS (Latmos Hybrid Simulation). In Section 3 we compare and validate our newly developed model with Venus Express observations during a quiet stable solar wind period before applying our model to BepiColombo 2nd flyby using input solar wind parameters provided by Solar Orbiter. In Section 4 we provide an estimate of the global atmospheric ion escape from Venus at solar minimum during BepiColombo's flyby. In Section 5 we conclude our study.

2. Simulation Model

The LatHyS code has already been developed and used to model several planetary environments such as Mercury, Mars, Titan, and Ganymede [Modolo et al., 2005, 2006, 2016, 2018; Richer et al., 2012; Leclercq et al., 2016]. The electromagnetic hybrid simulation treats ions kinetically by solving the Lorentz equation of motion, whereas electrons are treated as a mass-less charge-neutralizing fluid. The magnetic and electric fields are obtained by solving Maxwell's equations. The numerical scheme used in LatHyS for Venus is the same as the one used for the other planetary environments and described in Modolo et al. (2016). The coordinate system used is the Venus-Solar-Orbital (VSO)

system. The VSO X direction is taken along the Sun-Venus line, positive towards the Sun. The Z direction is parallel to the normal of the Venus orbital plane about the Sun, positive northward, and Y completes the right-handed coordinate system. All scales are in planetary radii, 1 Rv = 6052 km. The boundary conditions are the same as in Modolo et al. (2016), i.e., an open boundary is used in the X-direction while a periodic boundary is used in both the Y- and Z-directions. The Venus simulation consists of two species (protons and alpha particles) for solar wind plasma, three species (hydrogen, oxygen and carbon dioxide) for the neutral environment, and four species (H^+, O^+, O_2^+, CO_2^+) for ions of planetary origin. More details on the Venusian environment implemented in the code are given in the following subsections.

2.1 Exosphere

A steady-state exosphere including three main species at Venus (H, O, and CO_2) has been implemented in LatHyS.

Our hydrogen exosphere consists of hot and cold hydrogen atoms relying on the same profiles used in Kallio et al. (2006) and Jarvinen et al. (2016). The cold hydrogen population is modeled using a Chamberlain-type exospheric model [Chamberlain and Hunten, 1987; Bishop, 1990]:

$$n_{cold}(r) = n_0 e^{-\beta(1/r_0 - 1/r)} \xi(\frac{\beta}{r}), \beta = \frac{GM_v m_{H^+}}{k_B T} (1)$$

where r is the planetocentric distance, n_0 is the hydrogen density at $r = r_0$, and ξ the Chamberlain's partition function. The parameters used to describe β, i.e., G, Mv, m_{H^+}, k_B, and T are the gravitational constant, the mass of Venus, proton mass, Boltzmann's constant, and the temperature of the neutral species considered, respectively. The parameters n_0 and T are defined at two fixed Solar Zenith Angles (SZA), at noon (SZA = 0) and at midnight (SZA = 180), as summarized in Table 1. Linear interpolation is performed in order to model the dependence of the parameters with respect to SZA. In our simulation, ξ is set to unity.

The hot hydrogen population is modeled using inputs taken from Gunell et al. (2005) that are based on Rodriguez et al. (1984) that analyzed PVO observation. The corresponding profile is described by the function:

$n_{hot}(r) = e^{a_1 r + a_2 + a_3/r}$ (2)

where the three parameters a_1, a_2, a_3 are listed in Table 2. These three parameters are defined at three fixed SZA, at noon (SZA = 0), at the terminator (SZA = 90), and at midnight (SZA = 180). As done for the cold hydrogen population, a linear interpolation is performed in order to model the dependence of these three parameters with respect to SZA. The profile used in equation (2) is based on observations from Pioneer Venus Orbiter and compares nicely with the dayside Lyman-α observations obtained by Venus Express, as shown by Chaufray et al. (2012).

The oxygen exosphere also consists of both hot and cold populations. The cold oxygen population is modeled using equation (1) with inputs from Gunell et al. (2005) that are based on an analytical fit to the "standard case" of Mengel et al. (1989). In that case, n_0 and T are described by the functions

$n_0 = 10^{8.5+0.46cos(\theta)}$ (3),

$T = (314 - 44.1\theta^2)$ K when $\theta < 1.9284$ otherwise T is set to be 150 K (4),

where θ is the SZA in radian.

The hot oxygen population is modeled using equation (1) and the same approach as the one used for the cold hydrogen population [Kallio et al., 2006]. The corresponding parameters are summarized in Table 1.

Our cold carbon dioxide atom exosphere relies on a fit to the spherically-uniform profile shown in Fox and Sung (2001) (see Figure 1a in their paper) which is the result of the VTS3 model of Hedin et al. (1983). We consider the case of low solar activity since this is relevant to the time periods considered here for Venus Express as well as for the 2nd flyby of BepiColombo. The corresponding parameters are summarized in Table 1.

Altitude-dependent profiles of three exospheric neutrals at subsolar is shown in Figure 1,

Table 1. Numerical values of the parameters of equation (1) for the Chamberlain-type exospheric model used in the code. The Venus radius, Rv, is equal to 6052 km.

Species	SZA (deg)	n_0 [/cc]	T [K]	r_0 [km]	Reference
Cold Hydrogen	0	1.32×10^5	285	170+Rv	Rodriguez et al., 1984
	180	2.59×10^6	110	170+Rv	
Cold Oxygen	$0 < \theta < 180$	$10^{8.5+0.46\cos(\theta)}$	$314 - 44.1\theta^2$ 150 if $\theta > 1.9284$	170+Rv	Mengel et al., 1989; Gunell et al., 2005
Hot Oxygen	0	7.5×10^4	6400	200+Rv	McElroy et al. 1982
	180	2.0×10^3	4847	300+Rv	Nagy et al. 1981
Cold Carbon Dioxide	0 (combination of two profiles)	1.0×10^6	250	200+Rv	Hedin et al. 1983; Fox and Sung, 2001
		1.0×10^{11}	180	140+Rv	

Table 2. Numerical values of fitting parameters of equation (2) for the hot hydrogen exospheric population used in the code [e.g., Rodriguez et al. 1984; Gunell et al., 2005; Kallio et al., 2006].

Species	SZA (deg)	a_1	a_2	a_3
Hot hydrogen	0	-6.2625×10^{-5}	15.4817	3.6414×10^4
	90	-8.4607×10^{-5}	15.9944	2.9743×10^4
	180	-6.2309×10^{-5}	15.2723	4.3781×10^4

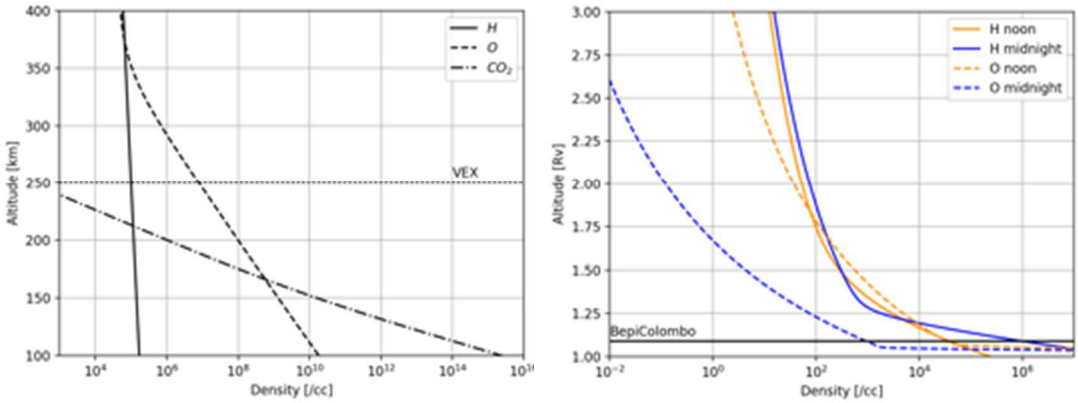

Figure 1. Altitude-dependent profiles of exospheric neutral densities (in cm^{-3}) consists of both hot and cold components. Left: for low altitudes (in km). Right: for high altitudes (in planetary radii, 1 Rv = 6052 km) at SZA = 0. The lowest altitude observed by BepiColombo during its second Venus flyby (550 km) is marked by a horizontal line in the right figure, and the lowest altitude during the nominal operation by VEX (250 km) is marked by a horizontal line in the left figure.

2.2 Ionosphere

The ionosphere is self-consistently calculated from the ionization of our exosphere. Four species are considered because they are the main components of the Venusian ionosphere [e.g., Fox and Sung, 2001]. Three sources of plasma are implemented in the code: photoproduction, charge exchange, and electron impact ionization. Details can be found in Modolo et al. (2016).

The local photoproduction rates of CO_2^+, O^+, and H^+ are calculated using the Extreme UltraViolet flux model for Aeronomics Calculations (EUVAC) developed by Richards et al. (1994) with the effect of the atmospheric photoabsorption. The F10.7 value is used as a proxy for solar activity, that is a solar flux measured in the 10.7 cm wavelength, and set to be 70, which corresponds to the value

observed by PVO and VEX at solar minimum [Masunaga et al., 2019]. F10.7 value is scaled up to the heliocentric distance at Venus location.

The production rate by electron impact ionization is calculated by:

$q_{X^+}^e = v_{X^+}^e n_X$ (5),

where $v_{X^+}^e$ is the electron impact coefficient rate that depends on the electron temperature T_e. In LatHyS, the electron impact coefficient rate is calculated by an exponential function with polynomial terms:

$v_{X^+}^e(T_e) = exp(A_0 + A_1 x + A_2 x^2 + A_3 x^3 + A_4 x^4)$ (6),

where $x = ln(T_e)$ and A_i are listed in Table 3 in Modolo et al. (2016).

The production rate by charge exchange is estimated from the following cross-sections, $\sigma_{H^+,H} = 2.5 \times 10^{-15}\ cm^2$, $\sigma_{H^+,O} = 1.0 \times 10^{-15}\ cm^2$, and $\sigma_{O^+,H} = 9.0 \times 10^{-16} cm^2$ [Stebbings et al. 1964; Stancil et al. 1999; Lindsay and Stebbings, 2005], and those are assumed to be constant.

In order to simplify the ionospheric description in our simulation, we have followed the same approach as the one used in LatHyS for the Martian environment [Modolo et al., 2016]. We focus here on the most important chemical reactions. For the Venusian environment, the parameters for the plasma ionization rates are taken from Schunk and Nagy (1980) and are the same as the ones used in Shinagawa et al. (1987) and Terada et al. (2002). Since the nitrogen exosphere is not implemented in LatHyS, six chemical reactions are solved in the simulation (see Table 3).

Reaction	Reaction rate constant [$cm^{-3}\ s^{-1}$]
$O^+ + CO_2 \rightarrow O_2^+ + CO$	9.4 x 10^{-10}
$CO_2^+ + O \rightarrow O_2^+ + CO$	1.64 x 10^{-10}
$CO_2^+ + O \rightarrow O^+ + CO_2$	9.6 x 10^{-11}

$H^+ + CO_2 \rightarrow CHO^+ + O$	3.0 x 10^{-9}
$CO_2^+ + e \rightarrow O + CO$	1.14 x $10^{-4}/T_e$
$O_2^+ + e \rightarrow O + O$	1.6 x $10^{-7}(300/T_e)^{0.55}$

Table 3. The chemical reactions implemented in the code together with their corresponding reaction rate constant. T_e is the electron temperature (in eV).

2.3 Solar wind input parameters

In LatHyS, the solar wind consists of both protons (95%) and alpha particles (5%). The solar wind density, velocity, proton temperature, and the Interplanetary Magnetic Field (IMF) are used as input parameters, and are steady in the simulation. In this study, we have made two different simulations. The first one, Run VEX, corresponds to one Venus Express orbit around Venus on May 17, 2009. The second one, Run BepiColombo, corresponds to the second Venus flyby by BepiColombo that occurred on August, 10 2021. A summary of the corresponding input parameters is shown in Table 4. Those input parameters are constrained by in situ magnetic field and charged particle observations obtained by Venus Express and by Solar Orbiter, respectively, as detailed in the next section.

Table 4: Summary of the solar wind input parameters used in our simulation runs.

	Run VEX	Run BepiColombo
Solar Wind density [/cc]	18	14.7
Solar Wind velocity [km/s]	335	338
IMF (Bx, By, Bz) [nT] in VSO	(3.2, -6.4, 10.5)	(-3.87, 6.2, -1.8)
Proton temperature [eV]	11	10.7

Plasma beta (proton)	0.49	1.1
Ion cyclotron frequency [/s]	1.216	0.726
Ion inertia length [km]	53.68	59.4
Alfven speed [km/s]	65.8	43.1
Alfven Mach number	5.1	7.8
Number of grids (Nx, Ny, Nz)	(300, 300, 300)	(423, 280, 280)
Simulation box [Rv]	($\pm$3.4, $\pm$3.4, $\pm$3.4)	(+2.6:-7.8, $\pm$3.4, $\pm$3.4)
Grid resolution [km]	134.2	147.9
Time step [Ω_i]	0.03	0.03

3. Results

3.1 Run VEX

In order to validate the newly developed global hybrid simulation LatHyS for the Venusian environment, we have first made a run with stable solar wind conditions constrained by Venus Express. We have selected one of the orbits where the difference in the IMF parameters between the inbound and outbound legs of VEX trajectory is small indicating the quiet solar wind and no events such as coronal mass ejections (see Table 4). Orbit number 1122 (May, 17 2009 with pericenter at 01:55:14 UT and at an altitude of 212.6 km) has been chosen. The VEX trajectory and observations from the magnetometer (MAG) [Zhang et al., 2006] and Analyze of Space Plasmas and Energetic Neutrals (ASPERA-4) plasma package [Barabash et al., 2007] are shown in Figure 2. The time resolution of the magnetic field data is 1s and that of electron and ion plasma data is 192s. VEX crossed the inbound bow shock at 01:35:22 UTC at a distance of 1.67 Rv. After that, before crossing

the inbound Ion Composition Boundary (ICB) at 01:50:00 UTC at a distance of 1.12 Rv, thermalized protons can be seen in IMA together with narrow energy spectra with a clear peak around 100 eV in ELS. Then inside the ICB, ELS observed ionospheric photoelectrons [e.g., Chong et al., 2018] around 30 eV. After crossing of the outbound ICB at 02:19:22 UTC and at a distance of 2.02 Rv, the spectra in both IMA and ELS is back to the solar wind energy showing that VEX was in the magnetosheath. The outbound bow shock crossing happaned at 04:35:33 UTC at a distance of 6.4 Rv.

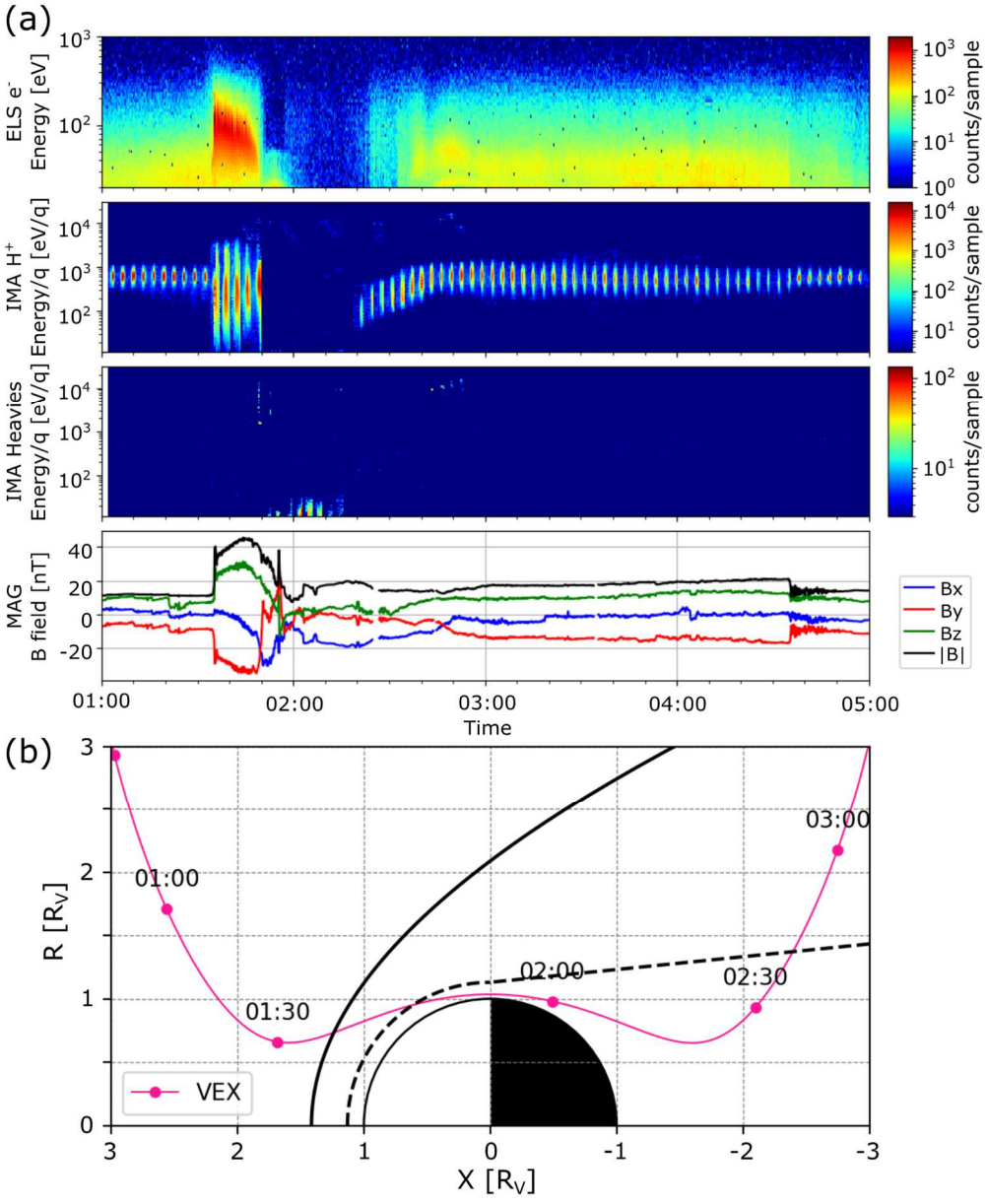

Figure 2. (a) Overview of VEX plasma and magnetic field observations on May, 17 2009. From top to bottom: energy-time spectrogram of electrons from the Electron spectrometer (ASPERA-4/ELS), proton and heavy ions from the Ion Mass Analyser (ASPERA-4/IMA), and magnetic field components

from MAG in VSO coordinates, versus time. The VEX/ASPERA-4/ELS instrument measures electron energy from 10 eV to 15 keV. The performances of the instrument are however different from its expected nominal response due to a misalignment of the inner hemisphere and a widening of the entrance aperture of the instrument [Collinson et al., 2009], hence only electron spectra above 20 eV are shown here since they cover the relevant electron populations discussed in our study. *The 192 s periodical cycle seen in the IMA data is due to the scanning cycle of the IMA elevation (Barabash et al., 2007). (b) VEX trajectory on the same day in cylindrical VSO coordinates. X connects the planetary center and the Sun;* $R = \sqrt{Y^2 + Z^2}$. *All scales are in planetary radii, 1 Rv = 6052 km. Both bow shock (solid black) and induced magnetosphere boundary (dashed-black) models refer to Martinez et al. (2008).*

Figure 3 shows the overview of the LatHyS simulation for Run VEX. The density distributions of the three ion species included in our simulation are shown together with the magnetic field lines. As expected, the IMF lines drape around Venus, an induced magnetosphere forms, which is partially filled with ions of planetary origin. We note that the planetary ions in our Venusian simulation are seen closer to the planet than in previous Martian simulations (see Modolo et al. (2006) for example) due to their smaller scale heights. Planetary protons are escaping mainly in the tail region while oxygen ions are escaping both in the dayside and tail region. Due to the larger Larmor radius of oxygen ions, an asymmetry of the ion escape in the Y-Z plane is noticeable. These ions follow the direction of the electric field [Barabash et al., 2007; Fedorov et al., 2011; Curry et al., 2015; Jarvinen et al., 2016; 2018]. Figure 4 shows the comparison between VEX observation and the virtual sampling in our LatHyS simulation for both plasmas and the magnetic field. The input parameters were taken around 01:00 UTC where the IMF is stable. In LatHyS, the bowshock is located a bit farther from the planet compared to the VEX observation, and large discrepancies in the magnetic field can be seen after 01:48 UTC. On another hand, a comparison between IMA observations and the virtual sampling of plasma in LatHyS shows good agreement, in particular for the proton observations. For heavy ions, the virtual sampling (4^{th} panel in Figure 4) shows some counts around

01:45 UTC, which coincide with the region where IMA shows the detaction of high-energy plasmas. Then low energy heavy ions are detected in IMA between two ion composition boundaries (ICB), which shows better agreement with the virtual sampling of protons (3rd panel in Figure 4) while the virtual sampling of oxygen ions show higher energy. The oxygen ions observed in LatHyS between 01:50 UTC and 02:10 UTC appear more energized compared to the real observations, and also the duration of the time interval when oxygen ions are observed in the virtual sampling is not as long as in the IMA observations. The discrepancies between in-situ observations and the virtual sampling will be further discussed in Section 4.1. Considering that the shock crossings and plasma spectra obtained in LatHyS along the trajectory in the inbound sectors, the general shape and magnitude of the observations are well grasped by the model with minimal differences. Thus, we consider that the LatHyS-Venus simulation is well validated and can be used with enough confidence for the 2nd Venus flyby of BepiColombo.

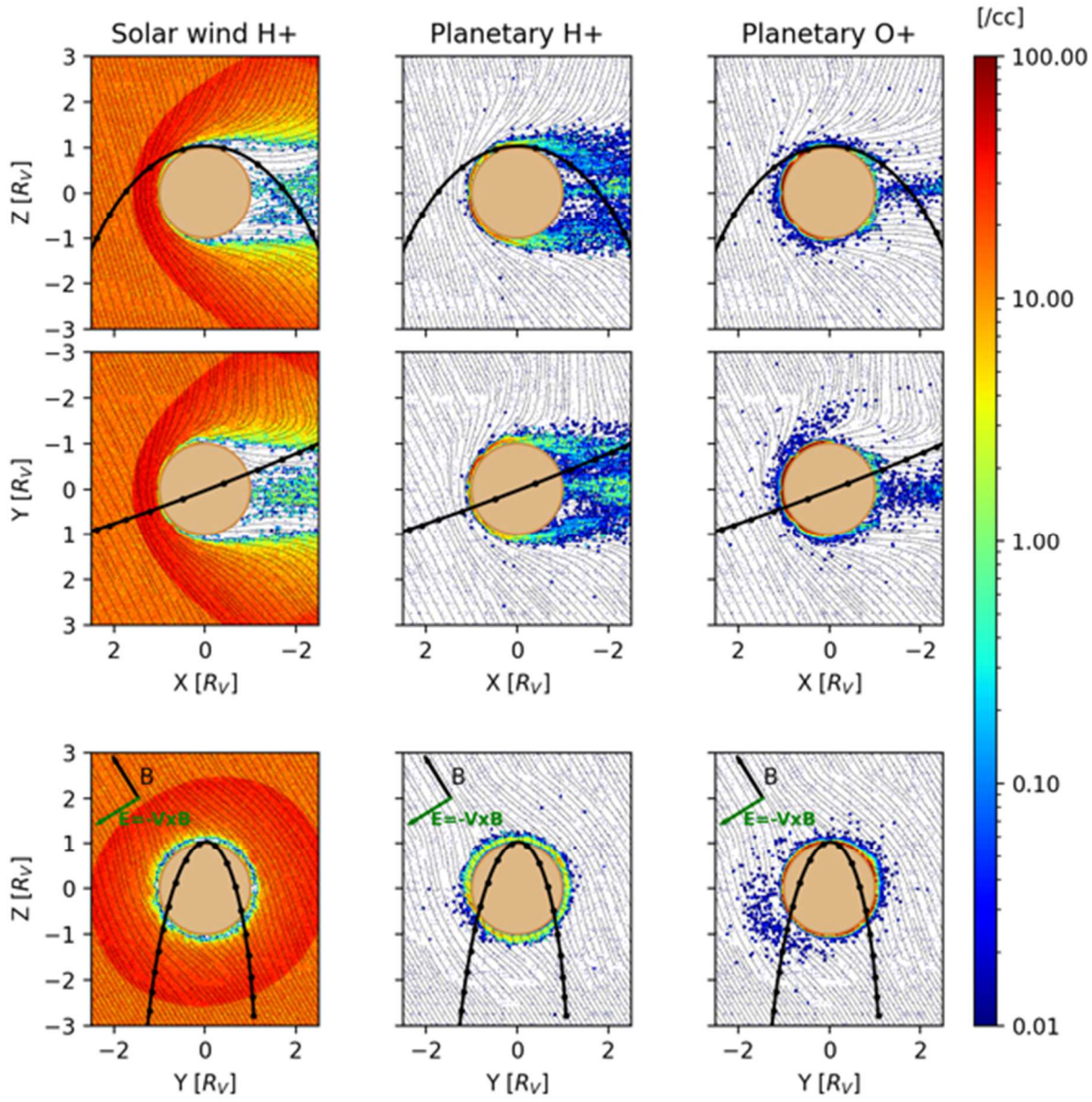

Figure 3. Overview of the LatHyS simulation for our Run VEX. The 2D colormap shows the solar wind proton, planetary proton, and planetary oxygen ion densities in the XZ, XY, and YZ (VSO) planes, with the magnetic field lines superimposed. The black line with the dots represents the VEX trajectory for Orbit number 1122. All scales are in planetary radii, 1 Rv = 6052 km, and the convection electric field is indicated by arrows in bottom figures.

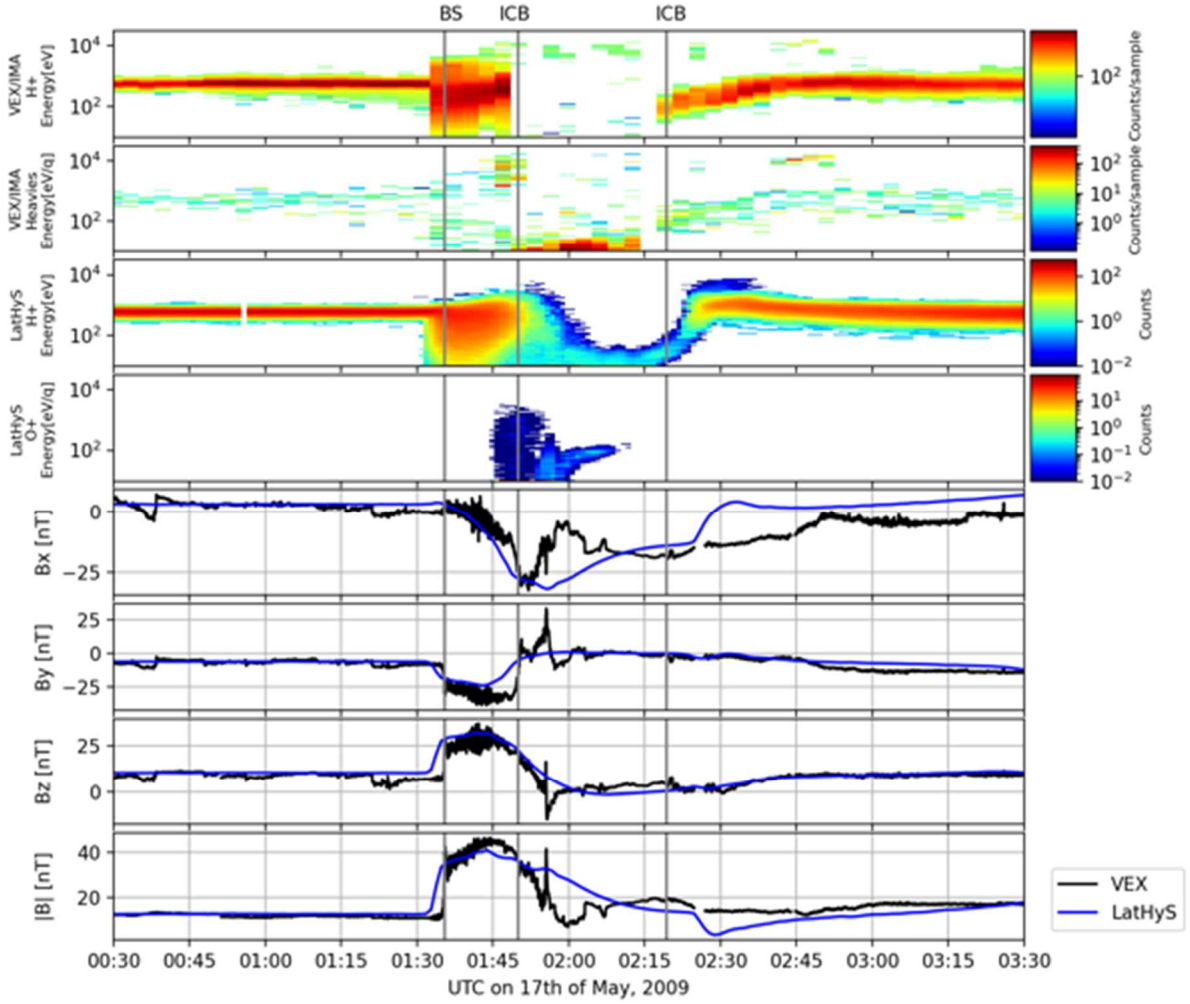

Figure 4. Comparison between the VEX observations and the virtual sampling in LatHyS for our Run VEX. From top to bottom, energy-time spectrogram of protons and heavy ions (counts per sample) observed by IMA onboard VEX, energy-time spectrograms of protons and oxygen ions (counts) virtually sampled in LatHyS, magnetic field components in VSO coordinate system, and magnitude (in nT), versus time (UTC). Three black vertical lines show the boundary crossings identified by the magnetic field from VEX observations: bowshock (BS) and Ion Composition Boundary (ICB).

3.2 Run BepiColombo

After having validated our newly developed global hybrid simulation LatHyS for the Venusian environment, we have made a second run for the 2nd flyby of BepiColombo which occurred

on August 10, 2021, with the closest approach at 13:51:54 UTC with an altitude of 552 km. During the closest approach, several instruments were turned on and obtained scientific data. In this study, we use the magnetic field data obtained by MPO-MAG [Heyner et al., 2021, Glassmeier et al., 2010], ion and electron data from Mercury Ion Analyzer (MIA) and Mercury Electron Analyzer (MEA) of Mercury Particle Plasma Experiment (MPPE) [Saito et al., 2021].

The corresponding BepiColombo trajectory, the magnetic field, and MPPE electron and ion plasma observations are shown in Figure 5. The time resolution of the magnetic field data is 1s and that of electron and ion plasma data is 4s. BepiColombo entered the Venusian induced magnetosphere on the nightside northern hemisphere from dusk to dawn. It crossed the last inbound bow shock around 13:00 UTC at a distance of 5 Rv and travelled along the plasma streamlines from the distant nightside to the close dayside Venusian magnetosheath before crossing the outbound bow shock at 14:01 UTC at a distance of 1.4 Rv (Persson et al., submitted). There were no indications from MPPE instruments onboard BepiColombo that it crossed the ion composition boundary during the whole flyby. However, the BepiColombo observations clearly show the change of plasma properties from nightside to dayside, including the crossing of the quasi-perpendicular bowshock at 14:01 UTC.

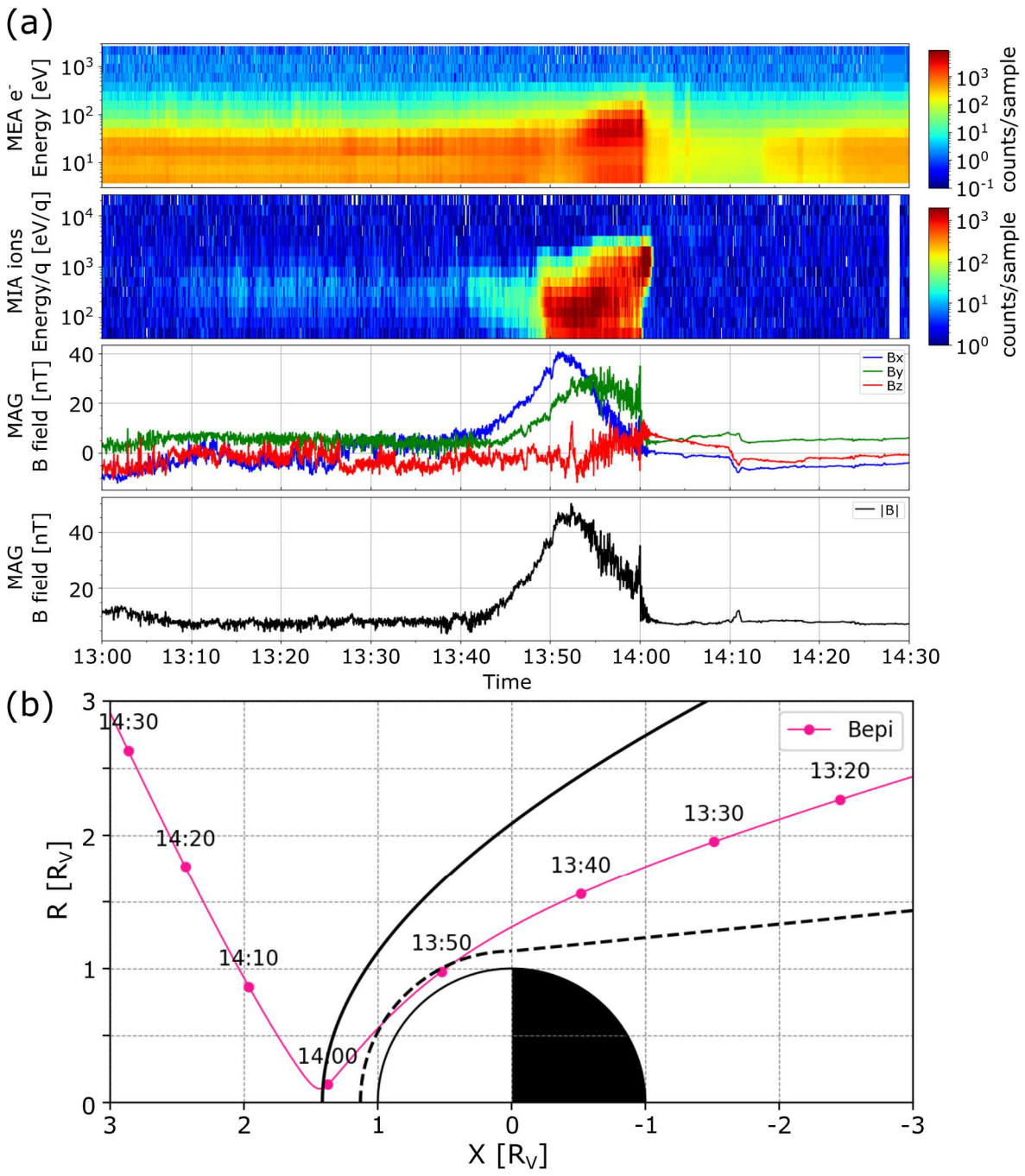

Figure 5. (a) Overview of electron and ion plasma and magnetic field measurements obtained by BepiColombo during its 2nd Venus flyby. From top to bottom: energy-time spectrogram of electron counts by MEA, energy-time spectrogram of ion counts by MIA, magnetic field components in VSO, magnetic field magnitude obtained by MPO-MAG, versus time. (b) BepiColombo trajectory on the same day in cylindrical VSO coordinates. The format is the same as Figure 2.

During the flyby, Solar Orbiter was located upstream of Venus at a distance of about 215 Rv (Figure 6(a)), and both spacecraft were located on the same Parker spiral which enables us to constrain very accurately our model run with solar wind parameters derived from observations by the Solar Orbiter magnetic field (MAG, Horbury et al., 2020) and plasma (Proton-Alpha Sensor (PAS), Owen et al., 2020) instruments. A careful comparison of magnetic field data from both Solar Orbiter and BepiColombo shows that the two measurements match (Pearson's correlation = 0.53, Spearman's correlation = 0.82) very well on a large scale – except when BepiColombo is within the induced magnetosphere of Venus – if a time shift of 1 hour, considering the distance between two spacecraft and solar wind, is taken into account (Figure 6(b)).

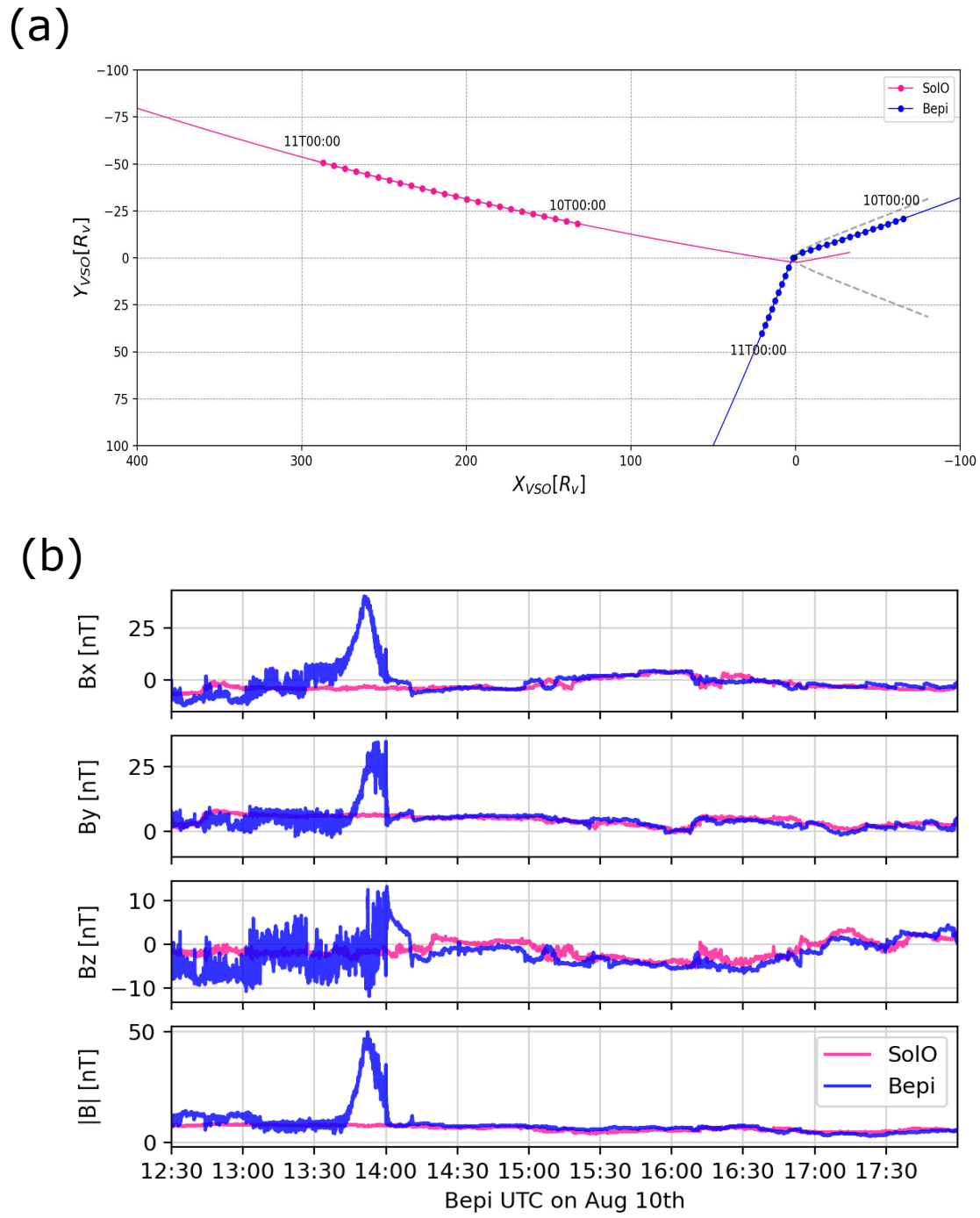

Figure 6. (a) Trajectories of Solar Orbiter (pink) and BepiColombo (blue) in the XY VSO plane on August, 10 2021. Distances are given in planetary radii, 1 Rv = 6052 km. The dots mark every one hour. (b) Comparison of the magnetic field observation between Solar Orbiter and BepiColombo. From top to bottom: BepiColombo magnetic field components in VSO coordinate system and magnetic field magnitude from BepiColombo MPO-MAG (in blue) and Solar Orbiter MAG (in black,

time-shifted by 1 hour), versus time (BepiColombo UTC on August, 10 2021, around BepiColombo's closest approach).

In addition, the solar wind observed by Solar Orbiter 1 hour before the closest approach of BepiColombo was remarkably stable (Figure 7), which provides accurate constraints for our simulation run. We, therefore, use time-averaged solar wind parameters measured by Solar Orbiter MAG and PAS during the time interval 12:45-13:10 UTC as incident input parameters (see Table 1).

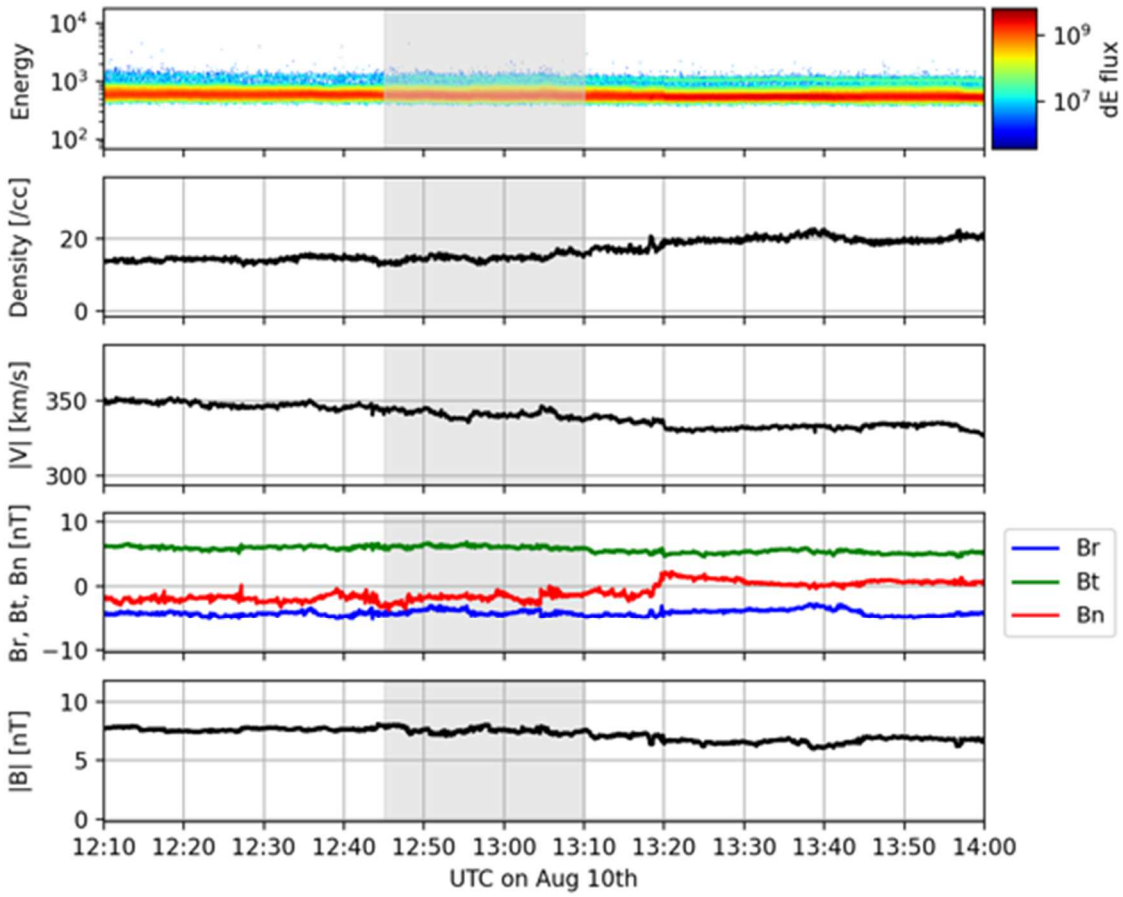

Figure 7. Overview of solar wind plasma and magnetic field measurements obtained by Solar Orbiter upstream of Venus from 12:10 UTC to 14:00 UTC on August, 10 2021 corresponding to the BepiColombo 2nd Venus flyby. The region marked by gray is the time period used (12:45-13:10 UTC) to derive the averaged solar wind parameters used to constrain the LatHyS simulation (see Table 1). During this time period, clearly the solar wind was stable. From top to bottom: energy-time spectrogram of ion differential energy flux (in cm^{-2} s^{-1} eV/eV), proton density (in cm^{-3}), proton bulk

speed (in km/s), magnetic field components (in nT) in RTN (Radial-Tangential-Normal) coordinate system, magnetic field magnitude, versus time (UTC on August 10, 2021).

Figure 8 shows the overview of the LatHyS simulation results for Run BepiColombo. The planetary oxygen ions are picked up like a plume [e.g., Dong et al., 2015] and the planetary protons are escaping down to the tail region. These plasma structures follow the direction of the electric field, but interestingly, the way they are escaping is different between oxygen ions and protons. Oxygen ions are clustered, detached, and escaping in the dayside, while protons are propagating towards the tail, and escaping as a tailward flow.

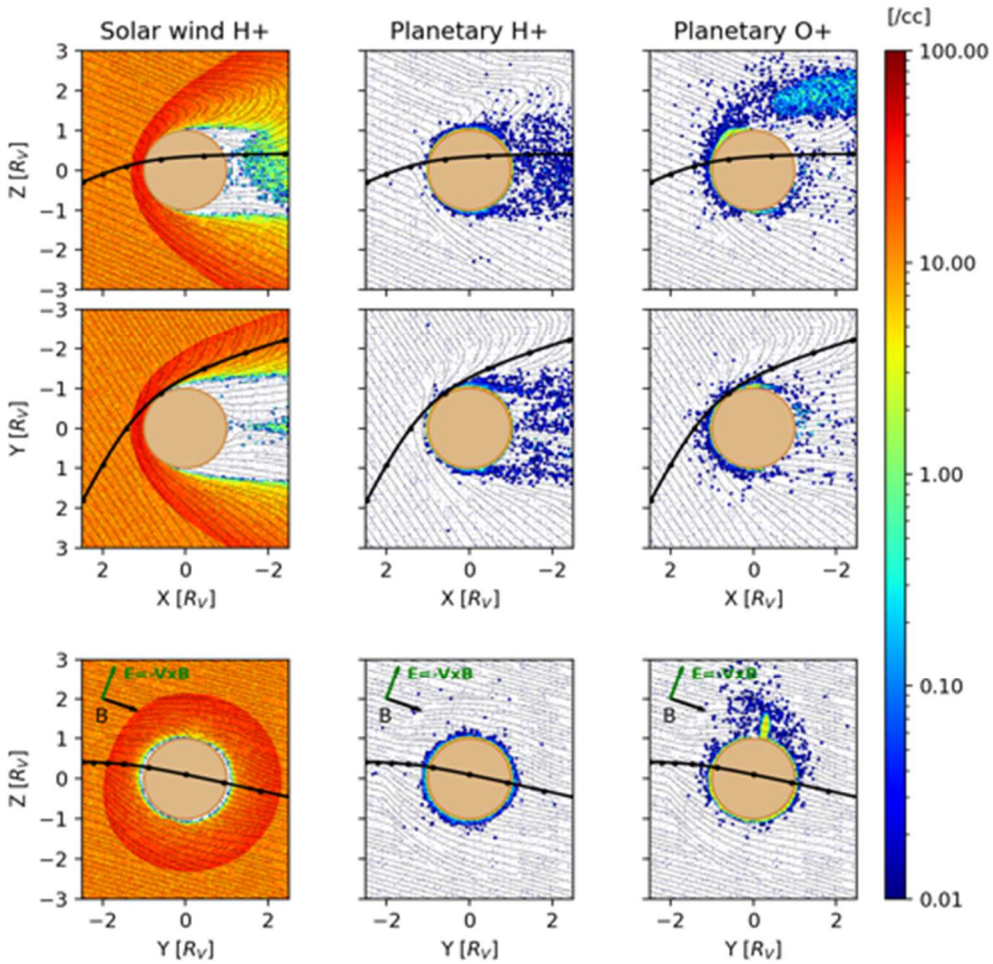

Figure 8. Outputs of the LatHyS simulation for Run BepiColombo. The format is the same as Figure 3.

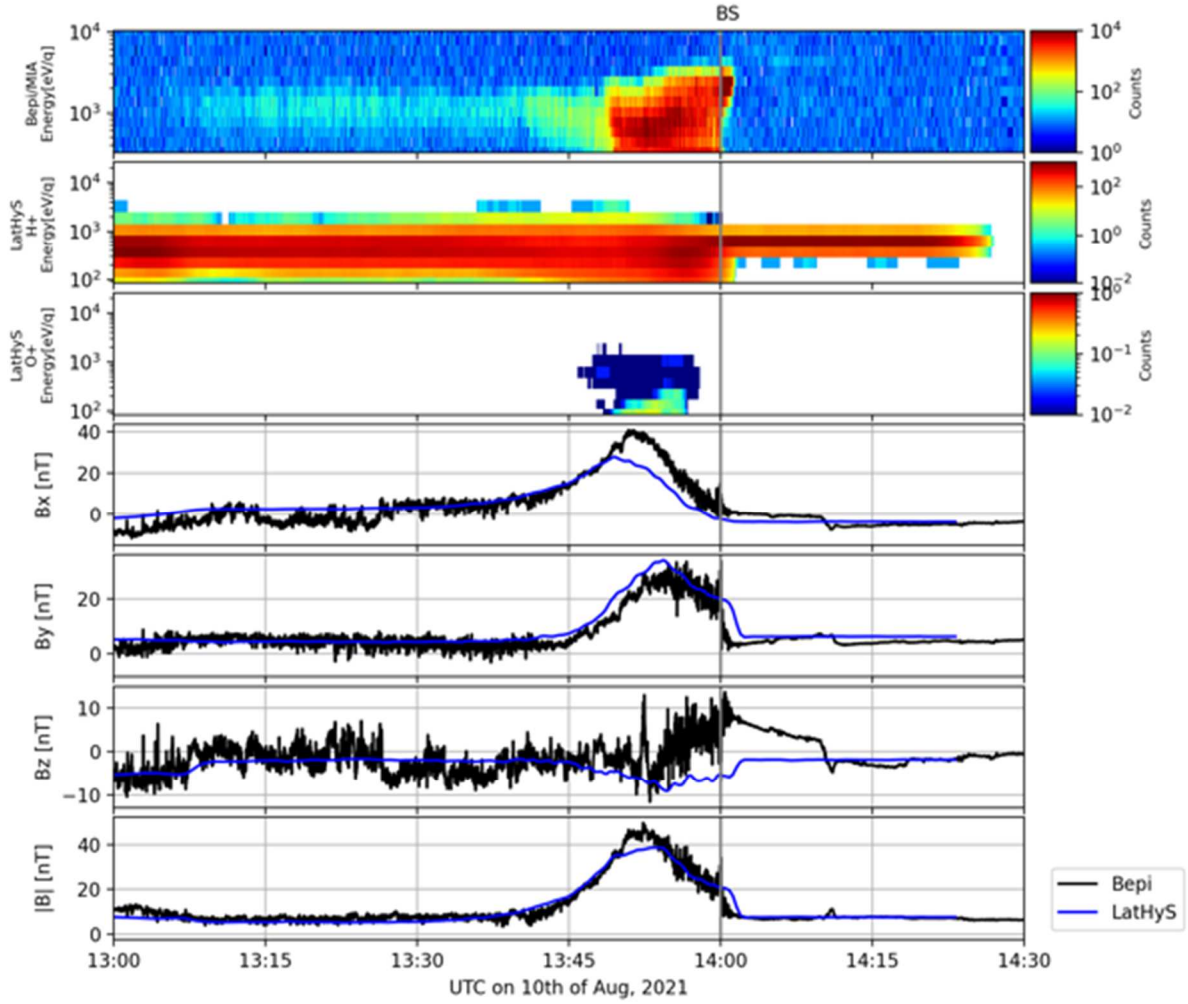

Figure 9. Comparison between the BepiColombo observations and the virtual sampling in LatHyS for our Run BepiColombo. From top to bottom, ion observation by MIA onboard BepiColombo, virtual sampling of protons and oxygen ions, magnetic field components, and magnitude versus time. The bowshock ramp (BS) is marked by a grey vertical line at 14:00 UTC.

Figure 9 shows a comparison between the BepiColombo observations and the virtual sampling in LatHyS for Run BepiColombo. The plasma sampling is made without any field of view constraints, thus, the proton simulation shows the solar wind component after 14:01 UTC. Then, when the spacecraft is around the closest approach (13:52 UTC), oxygen ions are sampled in LatHyS. The IMF is taken from the Solar Orbiter observation, thus it does not exactly match with each component of the magnetic field observed by BepiColombo in particular from 14:01 UTC to 14:18 UTC in the solar wind (Figure 9). However, the region between 13:00 UTC and 14:52 UTC the virtual sampling shows agreement with BepiColombo observations. This discrepancy is likely due to the input parameters taken from Solar Orbiter which fits better with BepiColombo observation in the longer interval but not short-time small variations. Moreover, a temporal variation of IMF configurations is not taken into account in the simulation.

4. Discussion

4.1 Discrepancies between simulations and observations

As shown in Figure 4, the inbound part for Run VEX is well reproduced by LatHyS, however, there is a large discrepancy after 01:45 UTC. This is simply due to the time-variable solar wind. Although we have selected the orbit which shows an almost similar IMF configuration between inbound and outbound solar wind observation, VEX takes 4 hours to complete one orbit. The solar wind changes in time, for example, at Mercury it takes only 20 minutes or even less to have a large change in the IMF cone/clock angle [James et al., 2017]. Thus, at Venus, we would expect to have several changes in the IMF configuration during one orbit [Benna et al., 2009]. In particular, at an unmagnetized planet like Venus, the IMF controls the induced magnetosphere which leads to that the direction of the convection electric field can change quickly when VEX is inside the induced magnetosphere, and thus, discrepancies may indicate a change in the solar wind configuration. The small discrepancy at the inbound bowshock between LatHyS and VEX could be due to (1) the small change in IMF at 01:20 UTC, (2) the limited spatial resolution used in the simulation, (3) the possible underestimation of solar wind plasma parameters by IMA observation [Fedorov et al., 2011]. The

comparison of plasma spectra also shows some discrepancies, however, this is also correlated to the discrepancies in the magnetic field. As mentioned in Section 3.1, the proton spectrum by IMA around 02:00 UTC does not match the virtual sampling. IMA did not detect protons, while LatHyS shows a certain number of protons close to the planet. This could be due to (1) solar wind variation in time, or (2) the simplified exosphere model used in the simulation, or (3) the limited field of view of IMA [Fedorov et al., 2011]. The spectrum of oxygen ions appears partially during the orbit, and the energy around 02:00 UTC is higher (~ 100 eV) than what IMA observed (~ a few tens of eV). In addition, there is a difference in the magnetic field observations between VEX and the virtual sampling in LatHyS of ~ 20 nT. A stronger magnetic field can lead to highly energized oxygen ions as it provides a stronger electric field along the gyration path, which may explain the difference between the observations and LatHyS. For instance, if we take a value of -10 nT for VEX and -30 nT for LatHyS as seen in Bx in the Figure 4 with the assumption of the same bulk velocity vector, the electric field calculated by $E = -V \times B$ is 3 times larger in LatHyS. Thus, the Lorentz force can lead to highly energized oxygen ions.

The magnetic field comparison for Run BepiColombo shows good agreement with observations, except for the Bz component. This is due to the small negative Bz component observed by Solar Orbiter, which is not consistent with the magnetic field observed by BepiColombo upstream to Venus. Although the upstream solar wind was stable, small time variation can lead to significant differences when they interact with the unmagnetized planet. Thus, it is clearly seen that the modeled (blue lines in Figure 9) and observed (black lines in Figure 9) magnetic field show good agreement from 13:00 UTC to 13:50 UTC, where BepiColombo was located a bit farther away from Venus. The high-frequency oscillations and perturbations in the magnetic field observed by BepiColombo are not well reproduced by LatHyS. This is because of the limited grid resolution and temporal variations that the model cannot reproduce. The grid resolution in the simulation for Run BepiColombo is ~ 148 km and considering the spacecraft speed around the closest approach (~ 12 km/s), we cannot reproduce oscillations or perturbations of less than ~ 12 seconds. During the cruise phase of BepiColombo, the Mio spacecraft is stuck inside a sunshield [e.g., Mangano et al., 2021] making the plasma observation difficult. Since only a few sectors are open to space [Saito et al., 2021], MIA cannot observe the solar

wind plasmas for example. Therefore, a virtual sampling with the limited field of view is compared with the observations and discussed. Figure 10 has the same format as Figure 9, but this time the 2nd and 3rd panels are the virtual samplings of plasmas with a limited field of view. The field of view information was taken from SPICE kernels (https://doi.org/10.5270/esa-dwuc9bs, version 281) and applied. The field of view was projected into the velocity distribution and particles inside the field of view were collected. When the field of view is limited, there are no oxygen ions sampled, and clearly, the solar wind is also not sampled. The part of the orbit when we have observed a significant number of protons matches well with MIA observations, however, we do not see the protons in the simulation from 13:10 UTC to 13:45 UTC. Moreover, just before the bow shock crossings around 14:00 UTC, the MIA spectrum displays an increase energy of the particles while the virtual sampling in LatHyS shows a more decreasing signature in energy. The possible reason why the high-energy populations around the bow shock is not seen could be the direction of the convection electric field. The high-energy protons around the bowshock are specularly the reflected ions gyrating along the convective electric field direction, typical for a quasi-perpendicular bow shock [Persson et al., 2022, submitted]. As explained above, actual observation around the bow shock shows a positive Bz component while LatHyS shows a negative Bz component, possibly due to a small change in the IMF. A change in sign of the Bz component is critical for the convection electric field. This discrepancy is due to the small difference between Solar Orbiter observations, which are used to constrain the model run and the BepiColombo observation, which are overall well-matched with BepiColombo observation but not perfectly, and or because the IMF changed with time.

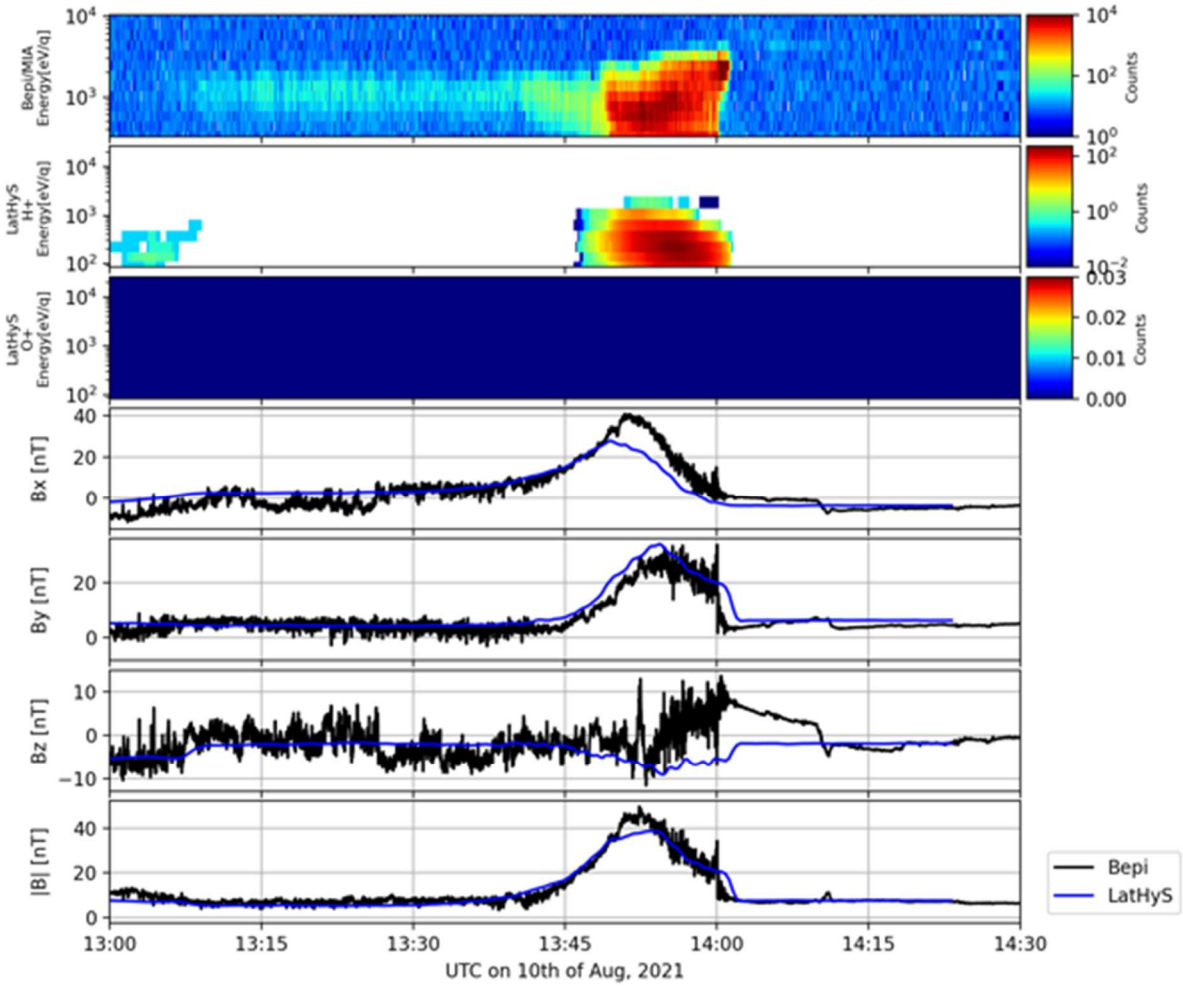

Figure 10. Comparison between the BepiColombo observations and the virtual sampling in LatHyS for our Run BepiColombo with the limited field of view for MIA. From top to bottom, ion observation by MIA onboard BepiColombo, virtual sampling of protons and oxygen ions (no oxygen ions in a given field of view), magnetic field components, and magnitude versus time.

4.2 Ion escape

One of the biggest questions to be addressed in general at unmagnetized planets is the ion escape variation following changing solar wind configurations. In this section, we discuss the ion escape for both Run VEX and BepiColombo. As discussed in section 3, planetary ions are escaping

by following the convection electric field and the distance reached by ions along the electric field direction is determined by their Larmor radius. When hydrogen and oxygen ions are picked up and get energized, they will reach the same energy. Due to their difference in mass, oxygen ions will have a Larmor radius 16 times larger than that of protons. For instance, in the case of Run VEX, the drift velocity in the solar wind is 324 km/s, and thus the Larmor radius for oxygen ions is ~4261 km (~ 0.7Rv), and for protons is 266 km [e.g., Jarvinen et al., 2018]. It means that once the oxygen is picked up in the dayside, they can immediately get energized and travel farther from the planet (seen as the plume) while protons are still concentrated close to the planet. Thus the protons travelling path are more along the planet than oxygen ions, and thus escape through the tail. Different escape channels (plume and tail escape) are common and have been reported by several authors [e.g., Dong et al., 2015; Jarvinen et al., 2016]. Figure 11 shows the 2D color map at X = -1.5 Rv for Run VEX. The clustered structure is due to the escape from dayside, and is seen in the negative electric field hemisphere. On the other hand, the distribution of planetary protons is more uniform with some enhancements in both negative and positive electric field hemispheres. Similar to the planetary species, the solar wind protons show similar asymmetry structure with concentration of ions in the negative electric field hemisphere and broader but enhanced distribution in the positive electric field hemisphere. These features are also seen in the VEX observations [e.g., Barabash et al., 2007]. The escape of oxygen ions at unmagnetized planets have been well studied by several authors regarding the dependence on the solar activity [Persson et al., 2018; 2020, Masunaga et al., 2019; Ramstad et al., 2015; Nilsson et al., 2021], solar wind configuration [Luhmann et al., 2007; Masunaga et al., 2011; Curry et al., 2015;], and how much both plume and tail escape contribute to the total ion escape [Dong et al., 2017]. Dong et al. (2017) has pointed out that the main source of the ion escape can be the tail escape at Mars and statistically 30% of total escape can come from plumes. In this study, Run BepiColombo shows a large plume and almost no tail escape while Run VEX shows the same amount of escape for both plume and tail escapes. Considering the solar wind parameter used in the study, the main difference may come from the cone angle, i.e., Run VEX has more perpendicular IMF to the Venus-Sun line, while Run BepiColombo has a more parallel configuration. Run BepiColombo suggests that the situation that plume escape is the dominant escape process is possible, but because of

the orbit bias and statistical analysis, it does not appear as a dominant source of ion escape. Moreover, the ion escape rate is calculated by calculating the escaping flux at the outer box for both Run VEX and Run BepiColombo. For planetary protons and oxygen ions (O^+), the escape rate is 6.9 x $10^{24}$and 4.7 x 10^{23} ions/s, respectively for Run VEX, 4.3 x 10^{24} and 4.2 x 10^{24}ions/s for Run BepiColombo. These values are the same magnitude or a bit low compared to the values previously reported (see Figure 20 in Futaana et al., 2017; the escape rates reported are in the range of 10^{23} – 10^{26}). This could be due to the simplified exosphere models used in the simulation. The exosphere models used are similar to those of Kallio et al. (2006) and Jarvinen et al., (2009) , with the exception of an injection of planetary plasmas from the inner boundary in these two later models while no injection in LatHyS.

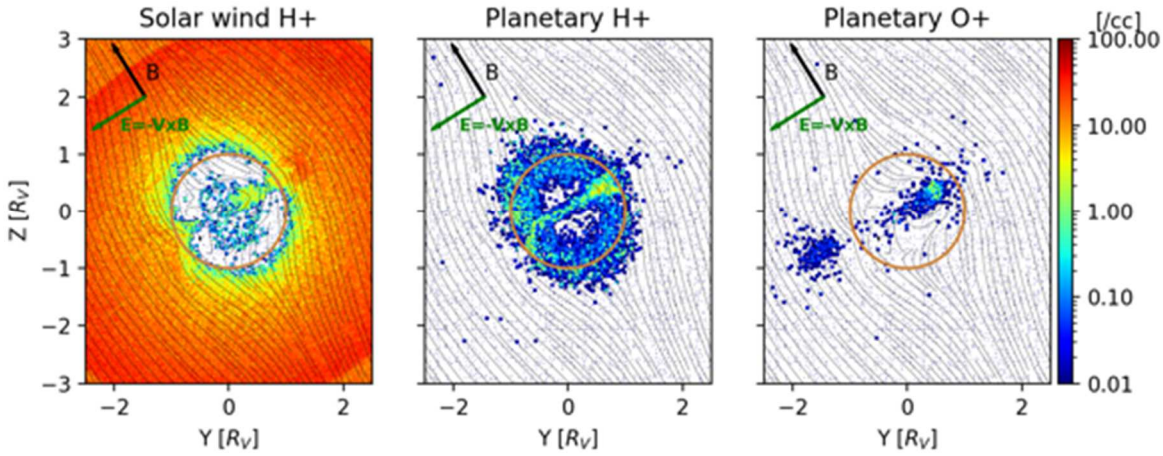

Figure 11. Outputs of the LatHyS simulations for Run VEX. The 2D colormaps show the solar wind proton, planetary proton, and planetary oxygen ion densities at X = -1.5 Rv, in the YZ VSO plane. The magnetic field lines are superimposed onto each 2D colormap. All scales are in planetary radii, 1 Rv = 6052 km. The circle represents the size of planet for reference.

5. Conclusions

The Venusian environment has been newly developed and implemented in the global hybrid simulation LatHyS, and we show the resulting model compared and validated with VEX observations. The LatHyS-Venus successfully reproduced the features observed by VEX, and showed consistent features of ion escape previously reported by several authors. Using LatHyS-Venus, the 2nd Venus flyby of BepiColombo has been studied and discussed for the first time, in particular, the observed signatures in the Venusian flanks are well reproduced in both magnetic fields and plasmas. The limited field of view of plasma instruments onboard BepiColombo was also taken into account in the simulation, and as a result, the most intense observed features have been properly captured in the LatHyS-Venus simulation, This shows that our simulation framework is a powerful tool to interpret and understand the in-situ data, especially when the spacecraft has a limited capability to access the full 3D ion distribution function of ions. Although global MHD simulations and global MHD with test particle tracing describe well the shock locations, global dynamics, and ion escape rates [e.g., Terada et al., 2009; Benna et al., 2009; Ma et al., 2013, 2020], hybrid simulations are necessary for the understanding of, in particular, the foreshocks and waves [e.g., Jarvinen et al., 2020]. The foreshock and waves give a different energization of picked up ions [e.g., Jarvinen et al., 2009; Brecht and Ledvina, 2021], that gives feedback to electromagnetic fields from particle behaviors (e.g., the effect of the ambipolar electric field or the electromagnetic field produced by the feedback from particles in the nightside region where the solar wind cannot penetrate into). The estimated ion escape rates are lower than the those observed by VEX, which could be due to the simplified exospheric models used. Implementing new features, such as multi-grid refinement to resolve exosphere with better spatial resolution, minor species components (e.g., nitrogen and carbon) in the Venusian environment, or even connecting it with the global circulation model are future tasks.

Acknowledgments. French co-authors acknowledge the support of CNES for the BepiColombo and Solar Orbiter missions. Sae Aizawa acknowledges the funding of the French National Research

Agency (ANR) for the TEMPETE (Temporal Evolution of Magnetized Planetary Environments during extreme Events) project. The simulation data used in this study are available at https://bepi-colombo.irap.omp.eu and can also be accessed through the 3Dview tool (http://3dview.cdpp.eu, Génot et al., 2020) developed by CDPP (http://cdpp.eu). The BepiColombo MEA data can be accessed through the Clweb tool developed at IRAP by Emmanuel Penou. The VEX magnetic field and plasma data used in this study are available in the Planetary Science Archive of the European Space Agency (https://archives.esac.esa.int/psa/). The Solar Orbiter magnetic field and plasma data used in this study are available at the Solar Orbiter Archive Repository (https://soar.esac.esa.int/soar/) of the European Space Agency. All these observational data are also available in the AMDA tool (https://amda.cdpp.eu, Génot et al., 2021) developed by CDPP, in particular the VEX solar wind ion plasma moments. Part of this work has benefited from the Sun Planet Interactions Digital Environment on Request (SPIDER) Virtual Activity of the Europlanet 2024 Research Infrastructure funded by the European Union's Horizon 2020 research and innovation programme under grant agreement No 871149. B.S.-C. acknowledges support through UK-STFC Ernest Rutherford Fellowship ST/V004115/1, and STFC grants ST/W00089X/1, ST/V000209/1. Solar Orbiter is a space mission of international collaborationbetween ESA and NASA, operated by ESA. Solar Orbiter Solar Wind Analyser (SWA) data are derived from scientific sensors which have been designed and created, and are operated under funding provided in numerous contracts from the UK Space Agency (UKSA), the UK Science and Technology Facilities Council (STFC), the Agenzia Spaziale Italiana (ASI), the Centre National d'Etudes Spatiales (CNES, France), the Centre National de la Recherche Scientifique (CNRS, France), the Czech contribution to the ESA PRODEX programme and NASA. Solar Orbiter SWA work at UCL/MSSL is currently funded under STFC grants ST/T001356/1 and ST/S000240/1. DH was supported by the German Ministerium für Wirtschaft und Energie and the German Zentrum für Luft- und Raumfahrt under contract 50 QW1501.

References

Allen et al., Energetic ions in the Venusian system: Insights from the first Solar Orbiter flyby, *Astronomy & Astrophysics*, 656, doi:10.1051/0004-6361/202140803, 2021

Barabash et al., The Analyser of Space Plasmas and Energetic Atoms (ASPERA-4) for the Venus Express mission, *Planetary and Space Science*, 55, doi:10.1016/j.pss.2007.01.014, 2007

Benna et al., Modeling the response of the induced magnetosphere of Venus to changing IMF direction using MESSENGER and Venus Express observations, *Geophysical Research Letters*, 36, doi:10.1029/2008GL036718, 2009

Brecht, S.H., and J.R. Ferrante, Global hybrid simulation of unmagnetized planets: Comparison of Venus and Mars, *Journal of Geophysical Research*, 96, doi:10.1029/91JA00671, 1991

Brecht, S.H., and S.A. Ledvina, An Explanation of the Nightside Ionospheric Structure of Venus, *Journal of Geophysical Research: Space Physics*, 126, 2, doi:10.1029/2020JA027779, 2021

Bishop, J., Analytic exosphere models for geocoronal applications, Planetary and Space Science, Volume 39, Issue 6, doi: https://doi.org/10.1016/0032-0633(91)90093-P, 1990

Cable, S. and R.S. Steinolfson, Three-dimensional MHD simulations of the interaction between Venus and the solar wind, *Journal of Geophysical Research*, Volume 100, doi:10.1029/95JA02174, 1995

Chamberlain, J.W. and D.M. Hunten, Theory of planetary atmospheres: An introduction to their physics and chemistry. (2nd edition). International Geophysics Series, 36. Academic Press Inc. Florida. 1987

Chaufray, J-Y, J-L Bertaux, E. Quémerais, E. Villard, and F. Leblanc, Hydrogen density in the dayside Venusian exosphere derived from Lyman-α observations by SPICAV on Venus Express, Icarus, 217, 767-778, doi: 10.1016/j.icarus.2011.09.027, 2012

Chong, G. S., Pope, S., Walker, S. N., Frahm, R. A., Zhang, T. L., & Futaana, Y. (2018). A statistical study of ionospheric boundary wave formation at Venus. Journal of Geophysical Research: Space Physics, 123, 7668–7685. https://doi.org/10.1029/2018JA025644

Collinson et al., Depleted Plasma Densities in the Ionosphere of Venus Near Solar Minimum From Parker Solar Probe Observations of Upper Hybrid Resonance Emission, *Geophysical Research Letters*, 48, 9, https://doi.org/10.1029/2020GL092243, 2021a

Collinson et al., A revised understanding of the structure of the Venusian magnetotail from a high-altitude intercept with a Tail Ray by Parker Solar Probe, Geophysical Research Letters, https://doi.org/10.1029/2021GL096485, 2021b

Curry, S. M., et al. (2015), Response of Mars O+ pickup ions to the 8 March 2015 ICME: Inferences from MAVEN data-based models, Geophys. Res. Lett., 42, doi:10.1002/2015GL065304

De Zeeuw et al., A new axisymmetric MHD model of the interaction of the solar wind with Venus, *Journal of Geophysical Research*, 101, doi:10.1029/95JE03363, 1996

Dong, Y., X. Fang, D. A. Brain, J. P. McFadden, J. S. Halekas, J. E. Connerney, S. M. Curry, Y. Harada, J. G. Luhmann, and B. M. Jakosky (2015), Strong plume fluxes at Mars observed by MAVEN: An important planetary ion escape channel, *Geophys. Res. Lett.*, 42, doi:10.1002/2015GL065346.

Dong, Y., X. Fang, D. A. Brain,J. P. McFadden, J. S. Halekas,J. E. P. Connerney, F. Eparvier,L. Andersson, D. Mitchell, andB. M. Jakosky (2017), Seasonal variability of Martian ion escape through the plume and tail from MAVENobservations,J. Geophys. Res. SpacePhysics,122, 4009–4022, doi:10.1002/2016JA023517

Fedorov, A., S. Barabash, J.-A. Sauvaud, Y. Futaana, T. L. Zhang, R. Lundin, and C. Ferrier (2011), Measurements of the ion escape rates from Venus for solar minimum, J. Geophys. Res., 116, A07220, doi:10.1029/2011JA016427

Fox, J.L. and K.Y. Sung, Solar activity variations of the Venus thermosphere/ionosphere, *Journal of Geophysical Research*, Volume 106, doi:10.1029/2001JA000069, 2001

Futaana et al., Solar Wind Interaction and Impact on the Venus Atmosphere, *Space Science Reviews*, 212, 3-4, 1453-1509, doi:10.1007/s11214-017-0362-8, 2017

Génot et al., Science data visualization in planetary and heliospheric contexts with 3DView, Planetary and Space Science, Volume 150, doi:10.1016/j.pss.2017.07.007, 2020

Génot et al., Automated Multi-Dataset Analysis (AMDA): An on-line database and analysis tool for heliospheric and planetary plasma data, Planetary and Space Science, Volume 201, doi:10.1016/j.pss.2021.105214, 2021

Gunell et al., Planetary ENA Imaging: Venus and a comparison with Mars, Planetary and Space Science, 53, doi:10.1016/j.pss.2004.07.021, 2005

Hadid et al., Solar Orbiter's first Venus flyby: Observations from the Radio and Plasma Wave instrument, Astronomy & Astrophysics, 656, doi:10.1051/0004-6361/202140934, 2021

Hedin et al., Global empirical model of the Venus thermosphere, Journal of Geophysical Research, Volume 88, doi:10.1029/JA088iA01p00073, 1983

Heyner et al., The BepiColombo Planetary Magnetometer MPO-MAG: What Can We Learn from the Hermean Magnetic Field?, Space Science Reviews, Volume 217, doi:10.1007/s11214-021-00822-x, 2021

Horbury et al., The Solar Orbiter magnetometer, Astronomy & Astrophysics, 642, doi:10.1051/0004-6361/201937257, 2020

Jarvinen et al., Hybrid modelling the Pioneer Venus Orbiter magnetic field observations, Advances in Space Research, 41, doi:10.1016/j.asr.2007.10.003, 2008

Jarvinen, R., Kallio, E., Janhunen, P., Barabash, S., Zhang, T. L., Pohjola, V., and Sillanpää, I.: Oxygen ion escape from Venus in a global hybrid simulation: role of the ionospheric O+ ions, Ann. Geophys., 27, 4333–4348, https://doi.org/10.5194/angeo-27-4333-2009, 2009.

Jarvinen, R., E. Kallio, and S. Dyadechkin, Hemispheric asymmetries of the Venus plasma environment, Journal of Geophysical Research: Space Physics, 118, doi:10.1002/jgra.50387, 2013

Jarvinen, R., D.A. Brain, and J.G. Luhmann, Dynamics of planetary ions in the induced magnetospheres of Venus and Mars, Planetary and Space Science, 127, doi:10.1016/j.pss.2015.08.012, 2016

Jarvinen, R., Brain, D. A., Modolo, R., Fedorov, A., & Holmström, M. (2018). Oxygen ion energization
at Mars: Comparison of MAVEN and Mars express observations to global hybrid simulation. Journal of Geophysical Research: Space Physics, 123, 1678–1689. https://doi.org/10.1002/2017JA024884

Jarvinen et al., Oxygen Ion Escape From Venus Is Modulated by Ultra-Low Frequency Waves, Geophysical Research Letters, 47, doi:10.1029/2020GL087462, 2020

Jin, H., K. Maezawa, and T. Mukai, The critical solar wind pressure for IMF penetration into the Venus ionosphere, Journal of Geophysical Research, Volume 113, doi:10.1029/2007JA012725, 2008

Kallio, E., J.G. Luhmann, and J.G. Lyon, Magnetic field near Venus: A comparison between Pioneer Venus Orbiter magnetic field observations and an MHD simulation, Journal of Geophysical Research, Volume 103, doi:10.1029/97JA02862, 1998

Kallio, E., R. Jarvinen, and P. Janhunen, Venus-solar wind interaction: Asymmetries and the escape of O^+ ions, Planetary and Space Science, Volume 54, doi:10.1016/j.pss.2006.04.030, 2006

Kallio et al., The Venusian induced magnetosphere: A case study of plasma and magnetic field measurements on the Venus Express mission, Planetary and Space Science, 56, doi:10.1016/j.pss.2007.09.011, 2008

Kallio, E., and R. Jarvinen, Kinetic effects on ion escape at Mars and Venus: Hybrid modeling studies, Earth, Planets and Space, Volume 64, doi:, 10.5047/eps.2011.08.014, 2012

Leclercq et al., 3D magnetospheric parallel hybrid multi-grid method applied to planet-plasma interactions, Journal of Computational Physics, Volume 309, doi:10.1016/j.jcp.2016.01.005, 2016

Lindsay and Stebbings, Charge transfer cross sections for energetic neutral atom data analysis, Journal of Geophysical Research: Space Physics, Volume 110, doi:10.1029/2005JA011298, 2005

Liu et al., Hybrid simulations of the O^+ ion escape from Venus: Influence of the solar wind density and the IMF x component, Advances in Space Research, 43, doi:10.1016/j.asr.2009.01.005, 2009

Luhmann, J. G., Kasprzak, W. T., and Russell, C. T. (2007), Space weather at Venus and its potential consequences for atmosphere evolution, J. Geophys. Res., 112, E04S10, doi:10.1029/2006JE002820.

Ma et al., A global multispecies single-fluid MHD study of the plasma interaction around Venus, Journal of Geophysical Research: Space Physics, Volume 118, doi:10.1029/2012JA018265 , 2013

Ma et al., Formation and Evolution of the Large-Scale Magnetic Fields in Venus' Ionosphere: Results From a Three Dimensional Global Multispecies MHD Model, Geophysical Research Letters, 47, doi:10.1029/2020GL087593, 2020

Mangano, V., Dósa, M., Fränz, M. et al. BepiColombo Science Investigations During Cruise and Flybys at the Earth, Venus and Mercury. Space Sci Rev 217, 23 (2021). https://doi.org/10.1007/s11214-021-00797-9

Martinecz et al., Plasma environment of Venus: Comparison of Venus Express ASPERA-4 measurements with 3-D hybrid simulations, Journal of Geophysical Research: Planets, Volume 114, doi:10.1029/2008JE00317, 2008

Masunaga, K., Futaana, Y., Yamauchi, M., Barabash, S., Zhang, T. L., Fedorov, A. O., Terada, N., and Okano, S. (2011), O+ outflow channels around Venus controlled by directions of the

interplanetary magnetic field: Observations of high energy O+ ions around the terminator, J. Geophys. Res., 116, A09326, doi:10.1029/2011JA016705.

Masunaga et al., Effects of the solar wind and the solar EUV flux on O^+ escape rates from Venus, Icarus, Volume 321, doi:10.1016/j.icarus.2018.11.017 , 2019

McElroy, M.B., M.J. Prather, and J.M. Rodriguez, Loss of oxygen from Venus, Geophysical Research Letters, 9, doi:10.1029/GL009i006p00649, 1982

McGray, J. E., and D. H. Pontius Jr., MHD simulations of boundary layer formation along the dayside Venus ionopause due to mass loading, Journal of Geophysical Research: Space Physics, Volume 99, Issue A2, doi: https://doi.org/10.1029/93JA03166, 1994

Mengel et al., Non-linear three dimensional spectral model of the Venusian thermosphere with super-rotation - I. Formulation and numerical technique, Planetary and Space Science, 37, doi:10.1016/0032-0633(89)90041-X,, 1989

Modolo et al., Influence of the solar EUV flux on the Martian plasma environment, Annales Geophysicae, vol. 23, doi:, 10.5194/angeo-23-433-2005, 2005

Modolo et al., Simulated solar wind plasma interaction with the Martian exosphere: influence of the solar EUV flux on the bow shock and the magnetic pile-up boundary, Annales Geophysicae, 24, doi:10.5194/angeo-24-3403-2006, 2006

Modolo et al., Mars-solar wind interaction: LatHyS, an improved parallel 3-D multispecies hybrid model, Journal of Geophysical Research: Space Physics, 121, doi:10.1002/2015JA022324, 2016

Modolo et al., The LatHyS database for planetary plasma environment investigations: Overview and a case study of data/model comparisons, Planetary and Space Science, 150, doi:10.1016/j.pss.2017.02.015, 2018

Murawski, K., and Steinolfson, R. S. (1996a), Numerical simulations of mass loading in the solar wind interaction with Venus, *J. Geophys. Res.*, 101(A2), 2547– 2560, doi:10.1029/95JA02433.

Murawski, K., and Steinolfson, R. S. (1996b), Numerical modeling of the solar wind interaction with Venus, Planetary and Space Science, volume 44, Issue 3, doi: https://doi.org/10.1016/0032-0633(95)00108-5

Nagy et al., Hot oxygen atoms in the upper atmosphere of Venus, Geophysical Research Letters, 8, 629, doi:10.1029/GL008i006p00629, 1981

Nilsson, H., et al., Solar cycle variation of ion escape from Mars, Icarus, doi : https://doi.org/10.1016/j.icarus.2021.114610, 2021

Owen et al., The Solar Orbiter Solar Wind Analyser (SWA) suite, Astronomy & Astrophysics, Volume 642, doi:10.1051/0004-6361/201937259, 2020

Persson, M., Y. Futaana, A. Fedorov, H. Nilsson, M. Hamrin, and S. Barabash (2018), "H+/O+ escape rate ratio in the Venus magnetotail and its dependence on the solar cycle". Geophysical Research Letters, doi: 10.1029/2018GL079454

Persson, M., Y. Futaana, R. Ramstad, K. Masunaga, H. Nilsson, M. Hamrin, A. Fedorov, and S. Barabash. (2020) "The Venusian Atmospheric Oxygen Ion Escape: Extrapolation to the Early Solar System". Journal of Geophysical Research: Planets 125, 3. https://doi.org/10.1029/2019JE006336.

Persson et al., BepiColombo's scenic tour reveals a large stagnation region at Venus, submitted

Ramstad, R., Barabash, S., Futaana, Y., Nilsson, H., Wang, X.-D., & Holmström, M. (2015). The Martian atmospheric ion escape rate dependence on solar wind and solar EUV conditions: 1. Seven years of Mars Express observations. Journal of Geophysical Research: Planets, 120, 1298–1309. https://doi.org/10.1002/2015JE004816

Richer et al., A global hybrid model for Mercury's interaction with the solar wind: Case study of the dipole representation, Journal of Geophysical Research, 117, doi:10.1029/2012JA017898, 2012

Richards, P. C., J. A. Fennelly, and D. G. Torr, EUVAC: A solar EUV flux model for aeronomic calculations, *J. Geophys. Res.*, 99(A5), 8981– 8992, doi:10.1029/94JA00518, 1994

Rodriguez et al., Hydrogen on venus: Exospheric distribution and escape, Planetary and Space Science, 32, doi:10.1016/0032-0633(84)90067-9, 1984

Saito et al., Pre-flight Calibration and Near-Earth Commissioning Results of the Mercury Plasma Particle Experiment (MPPE) Onboard MMO (Mio), doi:Space Science Reviews, Volume 217, doi:10.1007/s11214-021-00839-2, 2021

Schunk, R.W. and A.F. Nagy, Ionospheres of the terrestrial planets, Reviews of Geophysics and Space Physics, 18, doi:10.1029/RG018i004p00813, 1980

Shinagawa, H., T.E. Cravens, and A.F. Nagy, A one-dimensional time-dependent model of the magnetized ionosphere of Venus, Journal of Geophysical Research, 92, doi:10.1029/JA092iA07p07317, 1987

Slavin et al., MESSENGER and Venus Express observations of the solar wind interaction with Venus, *Geophysical Research Letters*, 36, doi:10.1029/2009GL037876, 2009

Stancil, P. C., D. R. Schultz, M. Kimura, J.-P. Gu, G. Hirsch, and R. J. Buenker, Charge transfer in collisions of O^+ with H and H^+ with O, *Astron. Astrophys. Suppl.*, 140, 225– 234, doi:10.1051/aas:1999419, 1999

Stebbings, R.F., A.C.H. Smith, and H. Ehrhardt et al., Charge Transfer between Oxygen Atoms and O^+ and H^+ Ions, Journal of Geophysical Research, 69, doi:10.1029/JZ069i011p02349, 1964

Tanaka, T., and Murawski, K. (1997), Three-dimensional MHD simulation of the solar wind interaction with the ionosphere of Venus: Results of two-component reacting plasma simulation, J. Geophys. Res., 102(A9), 19805– 19821, doi:10.1029/97JA01474.

Terada, N., S. Machida, and H. Teragawa, Global hybrid simulation of the Kelvin-Helmholtz instability at the Venus ionopause, Journal of Geophysical Research (Space Physics), 107, doi:10.1029/2001JA00922, 2002

Terada, N., H. Shinagawa, and S. Machida, Global hybrid model of the solar wind interaction with the Venus ionosphere: ion escape processes, Advances in Space Research, Volume 33, Issue 2, doi: https://doi.org/10.1016/j.asr.2003.05.011

Terada et al., A three-dimensional, multispecies, comprehensive MHD model of the solar wind interaction with the planet Venus, Journal of Geophysical Research: Space Physics, 114, doi:10.1029/2008JA013937, 2009

Volwerk et al., Solar Orbiter's first Venus flyby. MAG observations of structures and waves associated with the induced Venusian magnetosphere, Astronomy & Astrophysics, 656, doi:10.1051/0004-6361/20214091, 2021a

Volwerk et al., Venus's induced magnetosphere during active solar wind conditions at BepiColombo's Venus 1 flyby, Annales Geophysicae, Volume 39, Issue 5, doi:10.5194/angeo-39-811-2021, 2021b

Zhang et al., Magnetic field investigation of the Venus plasma environment: Expected new results from Venus Express, Planetary and Space Science, Volume 54, doi:10.1016/j.pss.2006.04.018, 2006